Rare Metal Materials and Engineering
Volume 53, Issue 9, September 2024
Available online at www.rmme.ac.cn

Science Press

Cite this article as: Chen Shuang, Yang Yanhong, Guo Zhiqiang, et al. Influence of Post-Treatment Process on Microstructure and Properties of Laser Additively Manufactured Nickel-Based Superalloy[J]. Rare Metal Materials and Engineering, 2024, 53(09): 2478-2484. DOI: 10.12442/j.issn.1002-185X.20230813.

ARTICLE

Influence of Post-Treatment Process on Microstructure and Properties of Laser Additively Manufactured Nickel-Based Superalloy

Chen Shuang[1,2], Yang Yanhong[2], Guo Zhiqiang[1], Liang Jingjing[2], Li Jinguo[2], Zhou Yizhou[2]

[1] School of Materials Science and Engineering, Shenyang University of Technology, Shenyang 110870, China; [2] Institute of Metal Research, Chinese Academy of Sciences, Shenyang 110016, China

Abstract: Defects such as cracks and micropores exist in nickel-based superalloy during laser powder bed fusion (LPBF), hindering their application in various fields. Hot isostatic pressing (HIP) was combined with conventional heat treatment (HT) to obtain LPBF nickel-based superalloy parts with ideal properties and fewer defects. The results show that HIP process can improve the densification, while the conventional HT can eliminate the micro-defects to improve the mechanical properties. After HIP treatment, the defect volume fraction of LPBF specimens decreases. After HT, the defect content of HIP+HT specimens increases slightly. After post-treatment, the hardness shows a decreasing trend, and the tensile strength and post-break elongation of HIP+HT specimens increase to 1326 MPa and 21.3%, respectively, at room temperature.

Key words: nickel-based superalloy; laser powder bed fusion; post-treatment; microstructure; properties

The rapid development of additive manufacturing technology has solved problems in rapid manufacturing of complex parts made of nickel-based superalloys[1–3]. In particular, the application of laser powder bed fusion (LPBF) technique realizes the direct manufacturing of nickel-based superalloy parts, which greatly improves the manufacturing efficiency of important parts in the fields of aerospace, petrochemical, medical and automotive manufacturing[4–7].

LPBF is a metal 3D printing technique based on high-energy laser beams[7–9]. The principle is to selectively melt and bond loose powders by heating the powder bed with concentrated energy scanning from a laser heat source[10–11]. This enables the molding of complex shaped parts[12–14]. Compared with traditional manufacturing methods, it overcomes the problems of long molding cycle time, poor molding quality, cumbersome post-processing, etc, and has the advantages of high molding density, good surface molding quality, high precision, etc. With high molding density and dimensional accuracy up to 20−50 μm, LPBF technique has a very high efficiency in the manufacture of metal parts[15–16].

LPBF produces defects (pores and cracks) during the manufacturing process, and these defects degrade the mechanical properties of the superalloy. In addition, due to the extremely high solidification rate of the alloy during the manufacturing process, high residual stresses are generated in the material. In order to eliminate the alloy defects and to improve its properties, different heat treatments (HTs) were used. Xuan et al[17] reported that single crystal superalloy was subjected to hot isostatic pressing (HIP) treatment, which resulted in an increase in mid-temperature plasticity. Microcracks disappear after HIP treatment, which increases the densification of the alloy. Baskov et al[18] investigated the effect of heat treatments such as HIP and HIP+solid solution+aging on EO741NP alloy. The post-treatment results in precipitation of γ' phase, dissolution of Laves phase and formation of *M*C carbide phase in the alloy. The mechanical

Received date: December 15, 2023
Foundation item: National Key R&D Program of China (2021YFB3700401); National Science and Technology Major Project (Y2019-VII-0011-0151); Science Center for Gas Turbine Project (HT-P2022-C-IV-002-001)
Corresponding author: Yang Yanhong, Ph. D., Associate Researcher, Institute of Metal Research, Chinese Academy of Sciences, Shenyang 110016, P. R. China, Tel: 0086-24-83971807, E-mail: yhyang@imr.ac.cn

properties of the alloy after HIP+solid solution+aging treatment were optimal. Roncery et al[19] carried out a suitable hot isostatic complete HT process on ERBO/1 alloy, which not only significantly reduced the number density of micropores, but also refined the microstructure of the γ/γ' phase in alloy, leading to an increase in the enduring creep life of the alloy at 750 °C/800 MPa. Sun et al[20] used a two-step HT method of HIP and solid solution to reduce micro-defects from 0.96% to 0.11%, which increased the tensile strength and elongation at break of the alloys at room temperature by 3.6% and 1135%, respectively, and increased the tensile strength and plasticity at 900 °C by 11.9% and 410%, respectively.

In this study, laser additive manufacturing of ZGH451 was researched and the effect of post-treatment (HIP, solid solution+aging and HIP+solid solution+aging) on the microstructure and mechanical properties of the alloy was analyzed. The alloys before and after post-treatment were characterized and their mechanical properties (hardness and tensile property) were compared.

1 Experiment

A laser additively manufactured nickel-based superalloy material, ZGH451, independently developed by the Institute of Metal Research, Chinese Academy of Sciences, was selected as the test material. Table 1 shows the chemical composition of the alloy. The LPBF experiments were carried out using a Concept Laser M2, equipped with a 400 W fiber laser on the SLM machine. In the multilayer addition stage, a 316L stainless steel plate was preheated and kept at a constant temperature of 100 °C. The working chamber was filled with argon gas, so the oxygen content was below 10 μL/L. Specific process parameters are shown in Table 2. The size of the resulting sample was 20 mm×20 mm×80 mm.

The specimens were investigated in four states i.e. LPBF, HIP, HIP+HT (solid solution+aging) and HT. HIP, HIP+HT and HT were firstly treated by stress relief annealing (650 °C/4 h, referred to as HT_0), followed by subsequent treatments. HIP parameters are 1200 °C/180 MPa/2 h; solid solution parameters are 1240 °C/3 h; aging parameters are: 1120 °C/4 h+850 °C/24 h.

The specimens were ground and polished by LAP-2MV metallographic grinding and polishing machine, respectively. Electrolytic corrosion was carried out on the finely polished samples, the corrosion solution was 15 g CrO_3+10 mL H_2SO_4+150 mL H_3PO_4, and the corrosion time was 15 s. The microstructures were observed by DM4M metallurgical microscope (OM) and SU8010 field emission scanning electron microscope (SEM), and the volume fractions of the micropores were calculated by the image analysis software Image-pro Plus. Electron backscattered diffraction (EBSD) analysis was also conducted. The residual stress of annealed specimens was tested with the LM-12 residual stress tester. Nanoindentation experiments were performed on the specimens by a Nano Indenter* G200 device at room temperature and the indenter was pressed down under 30 mN for 15 s. For the three-dimensional information (number, volume fraction and size) of the micropores inside the alloy, the specimens were quantitatively characterized by X-ray computed tomography (XCT, Versa XRM-500 device). The specimens used for XCT observation were cylindrical specimens with 2 mm in diameter and approximately 5 mm in height. The tensile properties of the specimens at the room temperature were tested by a TSE504D universal testing machine, and the tensile specimen is shown in Fig 1.

Table 1 Chemical composition of ZGH451 superalloy (wt%)

Ta+Mo+W	Al+Ti	Cr	C	Co	B	Ni
15.8	6.0	8.0	0.05	8.0	0.015	Bal.

Table 2 LPBF process parameters

Laser power/W	Speed /mm·s^{-1}	Spot size/μm	Focus movement/mm	Offset to original contour/mm
240	680	180	0	0.125

2 Results and Discussion

In order to prevent the excessive residual stress in the alloy due to deformation and cracking during post-processing, the laser additive manufacturing of nickel-based superalloy ZGH451 was firstly de-stressed and annealed, and the residual stress was reduced from 840 MPa to 744.6 MPa.

Fig. 2a–2b show the microstructures of LPBF specimens in the perpendicular and printing directions. In the LPBF specimens, overlapping "fish-scale" melt pools with a depth of 70 μm and a width of 110 μm can be observed. Microcracks of different sizes are randomly distributed at grain boundaries, which is similar to the microstructure of Hastelloy-X alloy prepared by LPBF[21]. At large magnification, columnar dendritic structures with different orientations can be observed, and this type of structure is also typical of other nickel-based superalloys prepared by LPBF[22–24].

Fig. 2c–2h show the microstructures of HIP, HIP+HT and HT specimens perpendicular to the printing direction. After the alloy is treated by the post-treatment process, the "fish-scale" melt pool boundary and the columnar dendritic structure with different orientations disappear, and the Ni_3Al-based γ' phase is precipitated in the nickel-based solid solution. After the HIP process (Fig. 2d), the γ' phase has

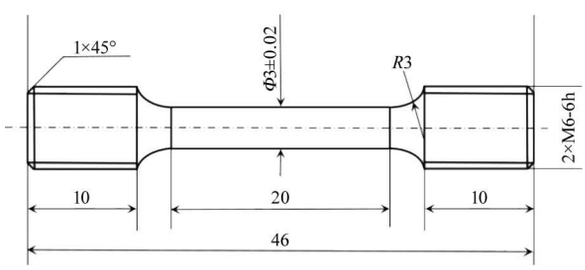

Fig.1 Schematic of tensile specimen

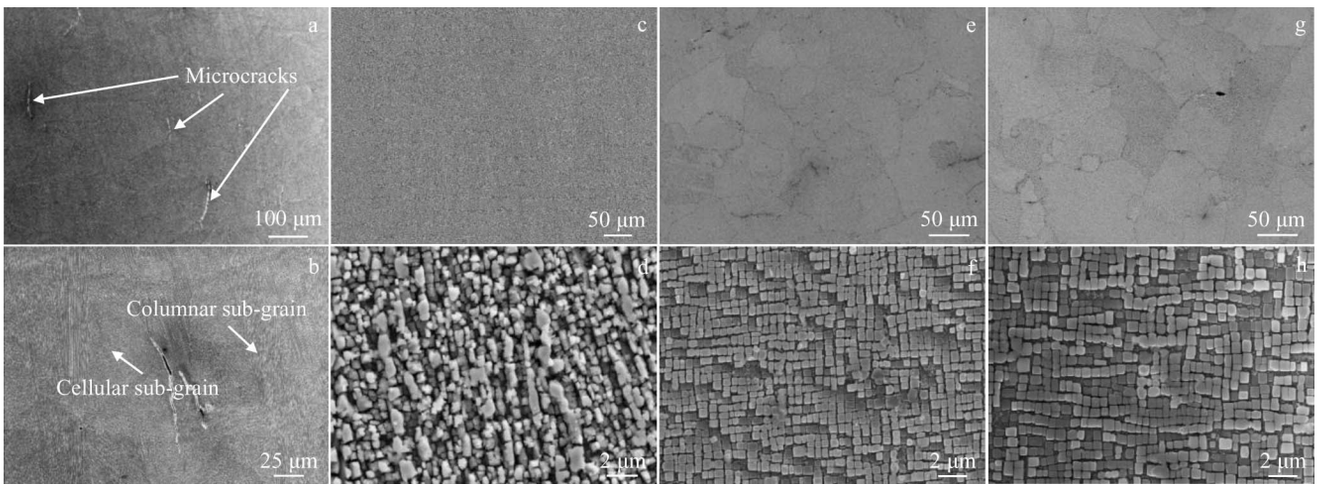

Fig.2 SEM images of nickel-based superalloy ZGH451 after different treatments: (a–b) LPBF, (c–d) HIP, (e–f) HIP+HT, and (g–h) HT

different sizes and irregular shapes, and a small part of the γ' phase is cubic. After HIP+HT and HT (Fig. 2e – 2h), the γ' phases are uniformly precipitated and cubic in shape, and it can be seen clearly that in the specimens treated by HIP+HT (Fig.2e–2h), the size of γ' phases is significantly reduced, with an average size of 0.533 μm and a high volume share of 60.9%.

Fig. 3 shows the EBSD results of LPBF specimens, HT_0 specimens, HIP specimens, HIP+HT specimens and HT specimens parallel to the printing direction. The columnar grain size of different specimens ranges from 5 μm to 400 μm, and the average grain size of LPBF specimen is 23.5 μm. The average grain sizes of HT_0 and HIP specimens are 25.7 and 27 μm, respectively, and the grain size, morphology and orientation are almost the same as those of LPBF specimen, indicating that there is no phenomenon such as recrystallization and grain growth during annealing and HIP. The average grain size of HIP+HT specimen is 60.4 μm, and grain morphology changes from columnar crystal to equiaxial crystal. The average grain size of HT sample is 71.3 μm. The grains of HIP+HT and HT specimens are mainly dominated by large grains, and the annealing twins can be observed, which indicates that the grains grow up and become coarse in the HT process.

As shown in Fig. 4 and Fig. 5, the microscopic defect contents of LPBF, HIP, HIP+HT and HT specimens are measured by OM and μ-CT analysis. Statistically, the OM and μ-CT densities in the samples are greater than 99.6%. It should be noted that due to the limitation of the specimen size and the number of specimens used in the experiments, OM observation is a two-dimensional detection and μ-CT is a three-dimensional detection, so the statistical results will be

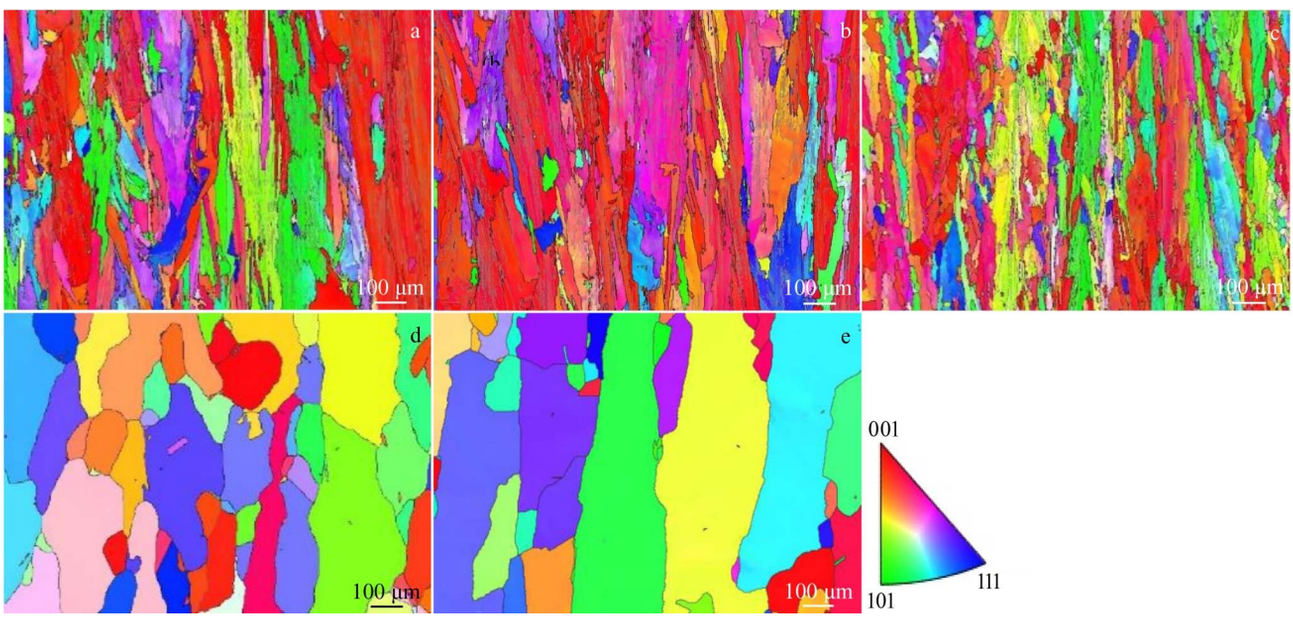

Fig.3 EBSD images of nickel-based superalloy ZGH451 after different treatments: (a) LPBF, (b) HT_0, (c) HIP, (d) HIP+HT, and (e) HT

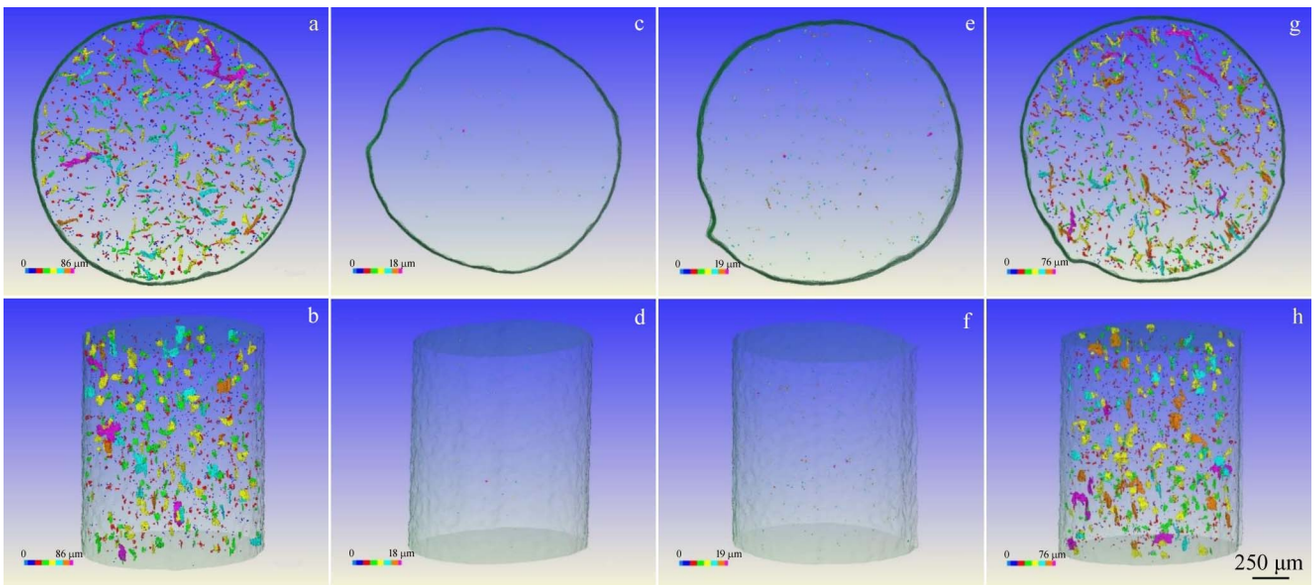

Fig.4 Morphologies and distribution of micropores in ZGH451 specimens after various treatments: (a–b) LPBF, (c–d) HIP, (e–f) HIP+HT, and (g–h) HT

somewhat different. As can be observed from Fig. 4, HT cannot improve the densification of the specimens, so the densities of the HT specimens and the LPBF specimens are close to each other. It can be clearly observed in Fig. 4c – 4f and Fig. 5d – 5i that the HIP process eliminates most of the defects and increases the specimen densities. From the OM and μ-CT plots, it can be observed that most of the pore morphology is spherical and near-spherical, which is consistent with the gas pores produced by the original powder particles[25–27]. After HIP+HT (Fig. 4e–4f), it can be found that the microcracks do not reappear, which suggests that there is no gas residue inside the microcracks. However, there is a slight increase in the micro-defects, which is attributed to the fact that the residual stress in the pores provides the impetus for the growth or regeneration of micropores during solid solution+aging, and an equivalent phenomenon was also found by Sun et al[20].

Fig. 6a – 6d show the nanoindentation load-displacement curves of the as-deposited specimens and the specimens with different HTs, under a peak load of 30 mN with six indentations (No. 1 – No. 6) for each specimen. As can be seen from Fig. 6a–6d, all the load-displacement curves are smooth, indicating that no "sawtooth rheological behavior" occurs, which is inconsistent with the phenomenon of heat-treated Hastelloy X and GH3536 alloys prepared by laser powder-bed melting[28–29]. Hastelloy X and GH3536 alloys undergo a significant "sawtooth rheological behavior" after HT. In general, the phenomenon of "sawtooth rheological behavior" (sudden displacement shifts) in the load-displacement curve of nanoindentation indicates that the mechanical behavior of the alloys changes from fully elastic deformation to plastic deformation. Each displacement shift corresponds to one or more shear zones which coordinate the plastic deformation of the material, and the larger the displacement shift, the more severe the shear plastic deformation inside the shear zone. As can be seen from Fig. 6, during the loading process, the stress-strain curve is smooth and upward, and there is no obvious displacement mutation or "sawtooth rheological behavior", indicating that no matter whether the deposited specimen is post-treated or not, the specimen is deformed by elastic deformation. This indicates that both the deposited and post-treated specimens mainly suffer elastic deformation.

Fig. 6e – 6f show the average hardness and the average elastic modulus of the as-deposited specimens and the specimens after different post-treatments obtained from the load-displacement curves. The hardness and elastic modulus of post-treated specimens are smaller than those of LPBF specimens, because after high-temperature treatment, the fine grains will be partly eliminated and partly transformed into recrystallization grains, in addition to the release of residual stresses in the material, which will lead to the reduction of hardness. The average hardness and average elastic modulus of HIP+HT specimens are higher than those of other specimens, probably because of the uniform precipitation of γ' and the reduced micro-defects.

Fig. 7 summarizes the stress-strain curves and tensile properties of ZGH451 alloy specimens in four different states. The tensile strength of the LPBF specimen is 1002.7 MPa and the elongation at break is 3.7%. The micro-defects in the specimen act as stress concentration areas under tensile loading, accelerating crack expansion and leading to premature fracture. The HT specimen has a tensile strength of 1276 MPa and an elongation at break of 12.1%, better than those of the LPBF specimen and the HIP specimen. The tensile strength of the HT specimen is 1326 MPa, and the elongation after break is 21.3%, significantly better than those of the LPBF, HIP and HT specimens. The HIP+HT specimen

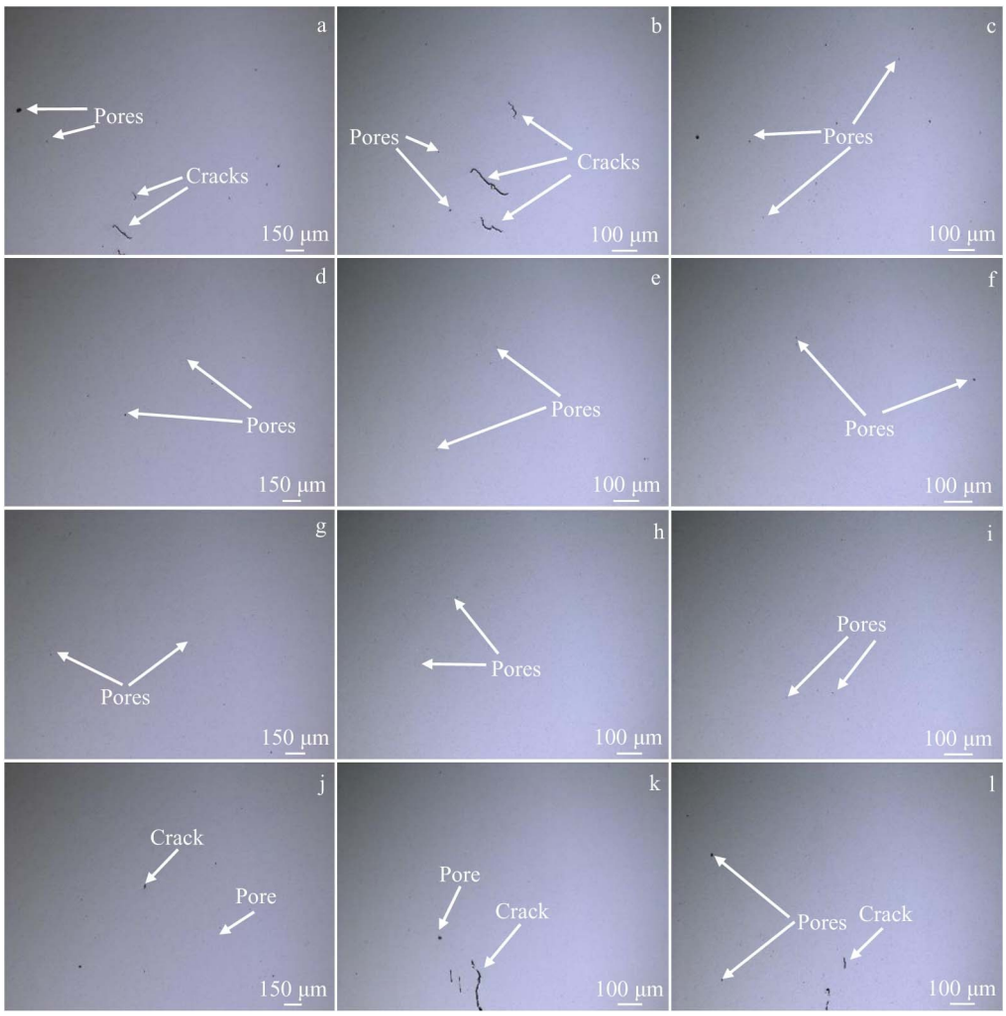

Fig.5 OM images of as-fabricated ZGH451 specimens obtained after various treatments: (a–c) LPBF, (d–f) HIP, (g–i) HIP+HT, and (j–l) HT

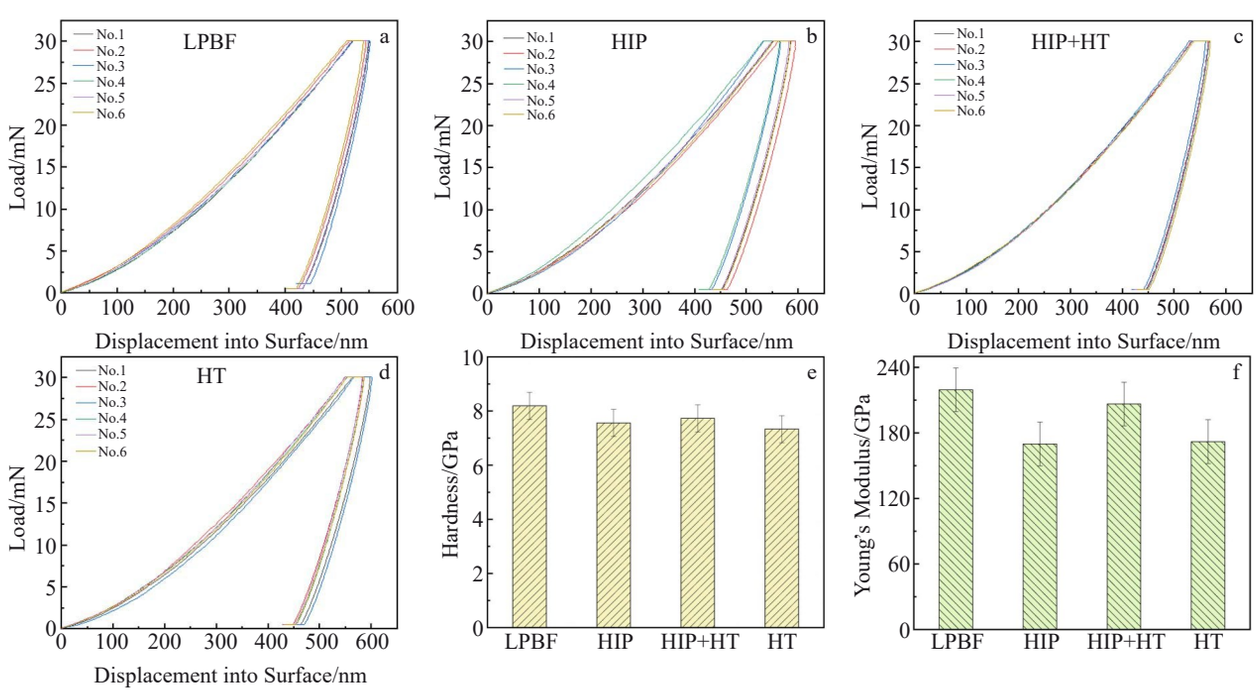

Fig.6 Load-displacement curves (a – d), hardness (e) and Young's modulus (f) of ZGH451 specimens after different treatments: (a) LPBF, (b) HIP, (c) HIP+HT, and (d) HT

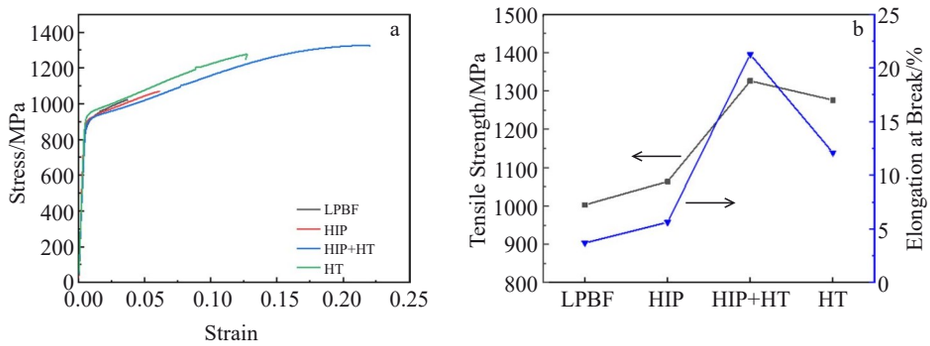

Fig.7 Stress-strain curves (a) and tensile properties (b) of ZGH451 specimens after different treatments

has a smaller size and a higher proportion of γ' phase. The HIP+HT specimen has a smaller size and a higher proportion of γ' phase. In addition, the reduction of grain size also increases the deformation resistance. After HIP treatment, the micro-defects are significantly reduced, and the tensile properties of the alloy are further improved.

3 Conclusions

1) After HIP treatment, the densification of LPBF specimens increases. After HT, the microscopic defects in HIP+HT specimens increase slightly compared with that in HIP specimens.

2) Because of higher dislocation density and larger residual stresses, LPBF specimens have the highest hardness, which decreases after post-treatment. With post-treatment, HIP+HT specimens have the highest hardness due to high volume share of γ' phase and higher densification.

3) At room temperature, the tensile strength and elongation at break of HIP+HT specimens increase to 1326 MPa and 21.3%, respectively, mainly due to the increase in densification, size reduction and increase in the volume share of γ' phase.

References

1 Geng Yaoxiang, Tang Hao, Luo Jinjie *et al*. *Rare Metal Materials and Engineering*[J], 2021, 50(3): 939 (in Chinese)

2 Zong Xuewen. *Rare Metal Materials and Engineering*[J], 2020, 49(9): 3182 (in Chinese)

3 Zhang Xue, Liu Changsheng. *Rare Metal Materials and Engineering*[J], 2021, 50(9): 3225 (in Chinese)

4 Jadhav A, Jadhav V S. *Materials Today: Proceedings*[J], 2022, 62: 2094

5 Zhao Y, Gong B, Wang Y *et al*. *Materials Science and Engineering A*[J], 2022, 858: 144133

6 Yang Xuanyi, Meng Qingshi. *Rare Metal Materials and Engineering*[J], 2021, 50(9): 3408 (in Chinese)

7 Wang Shaogang, Wang Sucheng, Zhang Lei. *Acta Metallurgica Sinica*[J], 2013, 49(8): 897

8 Wang Yifan, Yuan Xinbo, Che Qianying *et al*. *Titanium Industry Progress*[J], 2023, 40(6): 1 (in Chinese)

9 Mumtaz K A, Erasenthiran P, Hopkinson N. *Journal of Materials Processing Technology*[J], 2008, 195(1): 77

10 Panwisawas C, Tang Y T, Reed R C. *Nature Publishing Group*[J], 2020, 11(1): 2327

11 Dilberoglu U M, Gharehpapagh B, Yaman U *et al*. *Procedia Manufacturing*[J], 2017, 11: 545

12 Wang Fude. *The International Journal of Advanced Manufacturing Technology*[J], 2012, 58(5): 545

13 Gokuldoss P K, Kolla S, Eckert J. *Materials*[J], 2017, 10(6): 672

14 Ma P, Jia Y, Prashanth K G *et al*. *Journal of Alloys and Compounds*[J], 2016, 657: 430

15 Li N, Huang S, Zhang G *et al*. *Journal of Materials Science & Technology*[J], 2019, 35(2): 242

16 Vrancken B, Cain V, Knutsen R *et al*. *Scripta Materialia*[J], 2014, 87: 29

17 Xuan W, Zhang X, Zhao Y *et al*. *Journal of Materials Research and Technology*[J], 2021, 14: 1609

18 Baskov F A, Sentyurina Zh A, Kaplanskii Yu Yu *et al*. *Materials Science and Engineering A*[J], 2021, 817: 141340

19 Roncery M L, Lopez-Galilea I, Ruttert B *et al*. *Advanced Engineering Materials*[J], 2016, 18(8): 1381

20 Sun S, Teng Q, Xie Y *et al*. *Additive Manufacturing*[J], 2021, 46: 102168

21 Tomus D, Tian Y, Rometsch P A *et al*. *Materials Science and Engineering A*[J], 2016, 667: 42

22 Chlebus E, Gruber K, Kuźnicka B *et al*. *Materials Science and Engineering A*[J], 2015, 639: 647

23 Moussaoui K, Rubio W, Mousseigne M *et al*. *Materials Science and Engineering A*[J], 2018, 735: 182

24 Deng D, Peng R L, Brodin H *et al*. *Materials Science and Engineering A*[J], 2018, 713: 294

25 Shaji Karapuzha A, Fraser D, Zhu Y *et al*. *Journal of Materials Science & Technology*[J], 2022, 98: 99

26 Chauvet E, Kontis P, Jägle E A *et al*. *Acta Materialia*[J], 2018, 142: 82

27 Tillmann W, Schaak C, Nellesen J *et al*. *Additive Manufacturing*[J], 2017, 13: 93

28 Yuan Z, Chang F, Chen A *et al*. *Materials Science and*

Engineering A[J], 2022, 852: 143714

29 Bai Jie, Ma Rui, Wang Yajun *et al. Journal of Hebei Engineering University (Natural Science Edition)* [J], 2023, 40(3): 1062 (in Chinese)

后处理工艺对一种激光增材制造镍基高温合金组织与性能的影响

陈　爽[1,2]，杨彦红[2]，郭志强[1]，梁静静[2]，李金国[2]，周亦胄[2]

(1. 沈阳工业大学 材料科学与工程学院，辽宁 沈阳 110870)

(2. 中国科学院 金属研究所，辽宁 沈阳 110016)

摘　要：在激光增材制造过程中，镍基高温合金存在裂纹和微孔等缺陷，阻碍其在各领域应用。将热等静压（HIP）与传统热处理（HT）相结合，以获得缺陷少且性能理想的激光粉末床熔融（LPBF）镍基高温合金零件。结果表明，HIP工艺提高致密度，传统HT改善显微缺陷并提高力学性能。经HIP处理后，LPBF试样缺陷体积分数下降，经HT处理后，HIP+HT缺陷含量略有上升。经后处理后，硬度呈下降趋势，室温下，HIP+HT试样的抗拉伸强度和断后伸长率分别提高到1326 MPa和21.3%。

关键词：镍基高温合金；激光粉末床熔融；后处理；组织；性能

作者简介：陈　爽，女，1998年生，硕士，沈阳工业大学材料科学与工程学院，辽宁 沈阳 110870，E-mail：cs17824946735@163.com